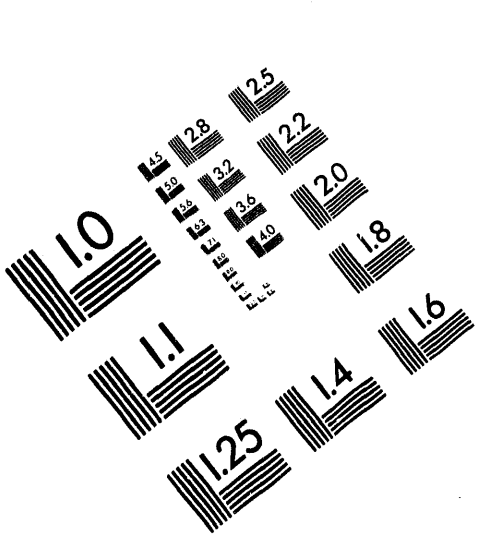

Association for Information and Image Management
1100 Wayne Avenue, Suite 1100
Silver Spring, Maryland 20910
301/587-8202

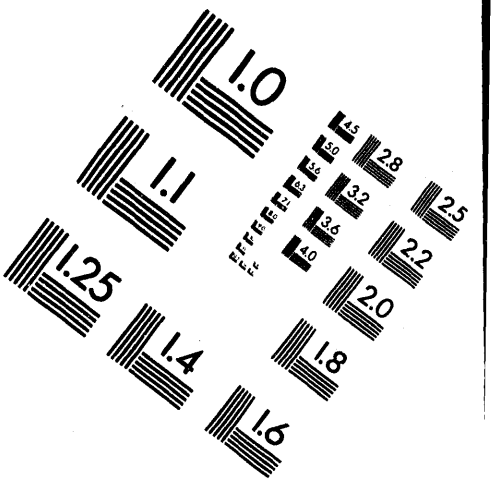

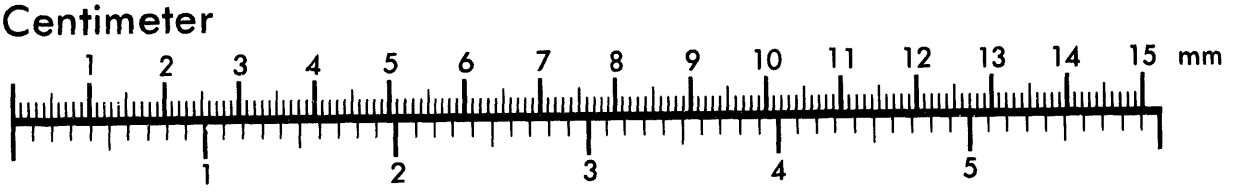

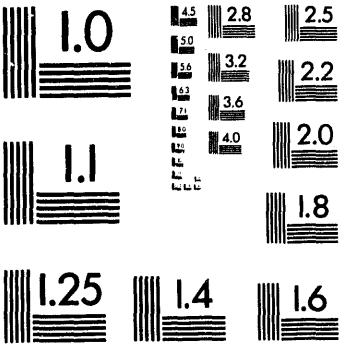

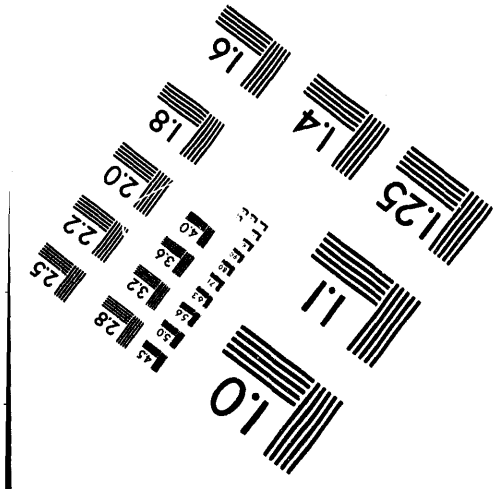

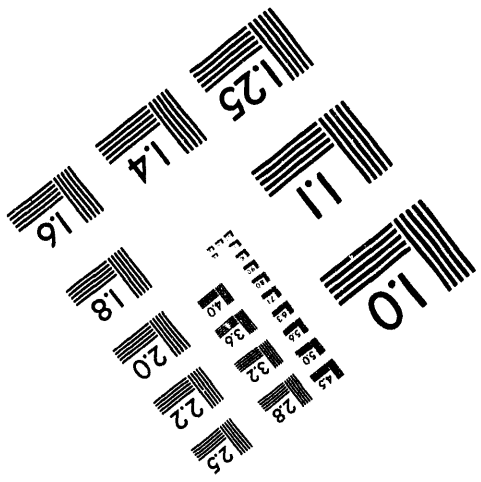

MANUFACTURED TO AIIM STANDARDS
BY APPLIED IMAGE, INC.

1 of 1

ANL/XFD/CP--80255
CONF-930824--10

Asymmetric-Cut Monochromator with Adjustable Asymmetry.*

R.K. Smither and P.B. Fernandez
Experimental Facilities Division
Advanced Photon Source
Argonne National Laboratory
Argonne Il 60439

January, 1993

CZ

*This work supported by the U.S. Department of Energy, BES Materials Sciences, under contract no. W-31-109-ENG-38

DISCLAIMER

Asymmetric-Cut Monochromator with Adjustable Asymmetry*

R. K. Smither and P. B. Fernandez
Advanced Photon Source
Argonne National Laboratory
Argonne, IL 60439

ABSTRACT

A variable-incident-angle, asymmetric-cut, double-crystal monochromator with adjustable asymmetry was tested at Argonne National Laboratory to evaluate its possible use on beamlines at the Advanced Photon Source (APS). For both undulator and wiggler beams, the monochromator can expand the area of the footprint of the beam on the surface of the crystals to 50 times the area of the incident beam. This increase in area will reduce the angular distortions of the crystalline planes by a factor of 2500. The asymmetric cut allows one to increase the acceptance angle for incident radiation and obtain a better match to the opening angle of the incident beam. This can increase the intensity of the diffracted beam by a factor of 2 to 5. The monochromator consists of two matched, asymmetric-cut (18 degrees) silicon crystals mounted so that they can be rotated independently about three different axes. Rotation around the first axis controls the Bragg angle. Rotation around the second axis controls the angle between the surface of the crystal and the horizontal plane of the beam and can make the footprint a rectangle with minimum length for this footprint area. The third rotation axis is perpendicular to the diffraction planes and carries the asymmetric-cut crystal. Rotation around this axis controls the amount of asymmetry being used and thus the increase of the area of the footprint of the beam on the crystal surface. The asymmetric cut is 18 degrees for the matched pair of crystals, which allows one to expand the footprint area by a factor of 50 for Bragg angles up to 19.15 degrees (6 keV for Si[111] planes). This monochromator, with proper cooling, will be quite useful for analyzing the high intensity x-ray beams produced by both undulators and wigglers at the APS.

*This work is supported by the U.S. DOE Contract No. W-31-109-Eng-38.

INTRODUCTION

A considerable amount of research effort has been expended at Argonne National Laboratory and at other synchrotron laboratories around the world to solve the high heat load problem that will exist at the new third-generation synchrotron sources.[1-5] The high heat load problem for the first optical component (diffraction crystal, multilayer, mirror, etc.) in the beamline is particularly severe for the new insertion device sources for which the x-ray beam flux per unit area and the total power will be 10 to 100 times that currently available.[6]

A number of partial solutions to this high heat load problem have been developed that improve the cooling of the first optical element, for example, Argonne has pioneered the use of liquid-metal cooling.[1-5]

After one has implemented the best cooling system possible, the most efficient way to further reduce the distortions of the surfaces of the first optical elements is to spread out the footprint of the x-ray beam. A novel geometry for a double-crystal monochromator has been developed at Argonne for undulator beams. This geometry spreads the x-ray beam on the surface of the crystal in a direction perpendicular to the beam direction and parallel to the horizontal axis of the beam.[5] This "high tilt" geometry has been tested and works well for undulator beams that are quite narrow in the horizontal direction, usually only a few millimeters wide, but does not work well for wiggler beams that tend to be much wider (2 to 6 cm). The work presented in this paper describes the design and preliminary lab tests of a double-crystal monochromator that will work well for both wiggler and undulator beams.

DESIGN AND SPECIAL FEATURES

The new double-crystal monochromator consists of two 18-degree asymmetric-cut silicon crystals, using the (111) planes. Each crystal can be rotated separately around three different axes, $\hat{\theta}$, $\hat{\Phi}$, and $\hat{\Psi}$, as shown in Figure 1. The angles θ, Φ, and Ψ correspond to rotations around the $\hat{\theta}$, $\hat{\Phi}$, and $\hat{\Psi}$ axes, respectively. (For clarity,

Figure 1 shows a square section of the round crystal that was used in the experiment.) In the lab experiment, the x-ray beam and the $\hat{\theta}$ axis are fixed in the lab frame. The $\hat{\theta}$ axis is always perpendicular to the direction of the incident x-ray beam and parallel to the horizontal plane of the beam. The $\hat{\Psi}$ axis is mounted on the θ stage so that it is always perpendicular to the $\hat{\theta}$ axis and in the direction of the x-ray beam when θ equals zero. The $\hat{\Phi}$ axis is mounted on the Ψ stage so that it is always perpendicular to the $\hat{\Psi}$ axis and perpendicular to the $\hat{\theta}$ axis when Ψ equals zero. The crystal is mounted on the Φ stage with its crystalline planes perpendicular to the $\hat{\Phi}$ axis. For $\Phi = 0$, both the crystalline planes and the crystal surface (their intersection is the neutral axis) are parallel to the $\hat{\Psi}$ axis, and the adjustable asymmetry is zero.

The symbols in Figure 1 are defined as follows: α_m is the asymmetric-cut angle (i.e., 18 degrees); α is the angle between the crystalline planes and the surface of the crystal in the plane defined by the beam direction vector and the $\hat{\Psi}$ axis; γ is the angle between the crystal surface and the beam direction in this same plane; θ is the rotation angle around the $\hat{\theta}$ axis, and, since this axis is perpendicular to the plane containing the beam direction and the $\hat{\Psi}$ axis, we find $\theta = \gamma + \alpha$; σ is the angle between the crystalline planes and the surface of the crystal in the plane defined by the $\hat{\Phi}$ axis and the $\hat{\theta}$ axis. Thus, the plane that contains σ is perpendicular to both the crystalline planes and the plane containing θ, α, and γ. Figure 1 shows the special case where $\Psi = 0$. In this case, the incident beam direction and the $\hat{\Psi}$ and $\hat{\Phi}$ axes are coplanar, and thus the plane defined by the direction of the beam and the $\hat{\Psi}$ axis coincides with the diffraction plane, which is vertical. Line A-A in Figure 1 is the intersection between either of these planes and the crystal surface. This line defines the edge of the footprint (crosshatched area) in the direction of the beam. Line A′-A′ is also on the surface of the crystal and defines the other edge of the footprint in the direction of the beam. Line B-B is the intersection between the plane defined by the direction of the beam and the $\hat{\Psi}$ axis (which for $\Psi = 0$ coincides with the

diffraction plane) and the crystalline plane. Line C-C is the intersection between the surface of the crystal and the plane containing the $\hat{\Phi}$ and $\hat{\theta}$ axes, while line D-D is the intersection between this same plane and the crystalline plane. Line C_S-C_S is the intersection between the surface of the crystal and the plane containing the surface normal $\hat{n}$ and the $\hat{\theta}$ axis. Both lines C-C and C_S-C_S are on the surface of the crystal.

The actual Bragg angle θ_B is related to θ by the relation $\sin\theta_B = \sin\theta \cos\Psi$. Thus $\theta = \theta_B$ when $\Psi = 0$, and the plane containing the beam direction and the $\hat{\Psi}$ axis coincides with the diffraction plane. Rotation around the $\hat{\theta}$ axis changes the Bragg angle θ_B between the incident x-ray beam and the crystalline planes and also the incidence angle γ of the beam on the surface of the crystal. Rotation around the $\hat{\Phi}$ axis changes the effective asymmetric cut of the crystal, α_B, which in turn changes the angle between the incident beam and the surface of the crystal. Therefore, rotation around the $\hat{\Phi}$ axis, which is perpendicular to the crystalline planes, changes the size of the footprint of the beam on the surface of the crystal without changing the Bragg angle in first order (see below). Rotation around the $\hat{\Psi}$ axis, which is perpendicular to the $\hat{\Phi}$ axis, changes the shape of the footprint and allows one to convert what is normally a parallelogram into a rectangle. With this type of shape control, it is possible to expand the footprint to the maximum area possible for any given crystal size.

As mentioned above, in the two-crystal monochromator tested in the laboratory, the $\hat{\theta}$ axis carries the $\hat{\Psi}$ axis, which in turn carries the $\hat{\Phi}$ axis. The crystal is mounted on the Φ stage with the crystalline planes perpendicular to the $\hat{\Phi}$ axis. Thus, the $\hat{\Phi}$ axis is always perpendicular to the crystalline planes, and, to first order, rotation around the $\hat{\Phi}$ axis does not change the Bragg angle θ_B. There is a small correction to θ_B that occurs as the effective asymmetric-cut angle, α_B, changes with a change in the rotation angle Φ. (α_B is the angle between the crystalline planes and the surface in the diffraction plane.) The $\hat{\Phi}$ axis is mounted on the Ψ rotation stage

in such a way that it is perpendicular to the $\hat{\Psi}$ axis. Therefore, as indicated above, the Bragg angle changes when Ψ is changed: $\sin\theta_B = \sin\theta \cos\Psi$. In most experiments, Ψ is fixed at an optimum angle during the experiment so the Ψ-θ_B dependence does not cause a problem.

The three rotation axes and their relation to each other were chosen for ease of alignment and operation of the monochromator; this choice is a special case of the many possible combinations. The salient features of our design are:

1. Variable beam footprint for high heat load applications: An increase in the area of the footprint by a factor 25 to 50 relative to the incident beam will reduce the slope errors, that is, the angular distortions of the crystalline planes caused by the heat in the x-ray beam, by a factor of 625 to 2500, respectively.

2. Variable acceptance: The angular and energy acceptance for each crystal can be adjusted for maximum throughput. An increase in the throughput of the monochromator of 2 to 5 can be achieved.

3. Reduced vertical walk: The vertical displacement of the output beam that occurs with a change in the Bragg angle is significantly reduced compared to the vertical walk of the output beam of a standard double-crystal monochromator.

EXPERIMENTAL SETUP

Figure 2 shows a schematic drawing of the variable-asymmetric-cut monochromator experimental setup. The x-ray source is on the left. The detector is on the right and has two positions: one for measuring the intensity of the beam diffracted off the first crystal with the second crystal removed, and one for measuring the intensity of the beam diffracted off the second crystal. Both crystals are cut with an asymmetric angle of 18 degrees and can be independently rotated about all three of the stacked axes: $\hat{\theta}$, $\hat{\Phi}$, and $\hat{\Psi}$. The second crystal can be moved toward or away from the first crystal. Some sideways displacement is also available for both crystals. The source is located 9 m from the first crystal. The vertical offset

is 9 cm. The vertical walk is controlled by moving the second crystal toward or away from the first crystal, and any horizontal walk caused by anything other than rotation around the $\hat{\Psi}$ axis is controlled by adjusting the angle Ψ. Only the Bragg angle needs to be adjusted with precision. The other two angles, Φ and Ψ, need to be adjusted much less accurately (0.5 degrees of arc). The asymmetric-cut crystals are 10 cm in diameter.

VARIABLE FOOTPRINT

The crosshatched area in Figure 1 is the footprint of the x-ray beam on the surface of the crystal. The area expansion ratio, R, is the ratio of the footprint area on the crystal surface to the cross-section area of the incident x-ray beam, and is given in the general case by the relation

$$R = -\frac{1}{(\hat{n} \bullet \hat{b})} ,$$

where $\hat{n}$ and $\hat{b}$ are the surface normal and the direction of the x-ray beam, respectively. In the special case shown in Figure 1, where $\Psi = 0$, R is given by

$$R = \frac{1}{\sin \gamma} \frac{\cos \alpha}{\cos \alpha_m} ,$$

where $\gamma = \theta - \alpha$, and is defined by the relationship $\tan \alpha = \tan \alpha_m \sin \Phi$. The $1/\sin \gamma$ term gives the increase in the length of the projection of the vertical edge of the beam on the surface relative to the beam height H. This projected length is labeled L_0 in Figure 1 and is given by

$$L_0 = \frac{H}{\sin \gamma} .$$

The term $(\cos \alpha / \cos \alpha_m)$ gives the increase in the projected width of the footprint, labeled W_f in Figure 1, relative to the beam width W:

$$W_f = W \frac{\cos \alpha}{\cos \alpha_m} .$$

The length L_S is the increase in the length of the footprint along the direction of the beam, due to the slanted side of the parallelogram-shaped footprint. The value of L_S

is given by

$$L_S = W \frac{\cos \alpha}{\tan \gamma} \tan \sigma \ ,$$

where $\tan \sigma = \tan \alpha_m \cos \Phi$. The length L_S is measured along line A′-A′ and extends from the corner of the footprint to the line C_S-C_S.

Figure 3 shows the general case when Ψ is not equal to zero. The definitions of the symbols are the same as in Figure 1. Note that the $\hat{\theta}$ axis no longer coincides with the line D-D, which is in the crystalline plane, and that the beam direction vector is no longer in the plane defined by the $\hat{\Phi}$ and $\hat{\Psi}$ axes. The ratio of the area of the footprint to the area of the beam is now given by

$$R = \frac{1}{\sin \gamma} \frac{\cos \alpha}{\cos \alpha_m} \frac{\cos \sigma}{\cos (\sigma - \Psi)} \ ,$$

where $\tan \alpha$ is now given by

$$\tan \alpha = \tan \alpha_m \sin \Phi \frac{\cos \sigma}{\cos (\sigma - \Psi)} \ .$$

As in the special case of $\Psi = 0$, we have $\gamma = \theta - \alpha$ and $\tan \sigma = \tan \alpha_m \cos \Phi$. The projection of the height of the beam on the crystal surface, L_0, is given as before by

$$L_0 = \frac{H}{\sin \gamma} \ ,$$

and W_f is given by

$$W_f = W \frac{\cos \alpha}{\cos \alpha_m} \frac{\cos \sigma}{\cos (\sigma - \Psi)} \ .$$

The extra length added by the slanting sides of the parallelogram-shaped footprint, L_S, is now

$$L_S = W \frac{\cos \alpha}{\tan \gamma} \tan (\sigma - \Psi) \ .$$

By adjusting $\Psi = \sigma$, we can make $L_S = 0$ and minimize the length of the footprint in the direction of the beam.

Figure 4 shows some results obtained at Argonne with a 4-mm-high and

12-mm-wide x-ray beam with an energy of 8 keV (θ_B = 14.2°), as one changes Φ and Ψ. Note that θ changes when Ψ changes, since $\sin\theta_B = \sin\theta \cos\Psi$. The shape of the footprint of the beam on the crystals was measured by exposing Polaroid film on the surface of the second crystal. The second crystal was used because the incident angle of the x-ray beam was much larger on the second crystal than on the first crystal when the expansion of the footprint was large. The error in the values of Φ and Ψ is ± 1°. Much of this error is due to the uncertainty in the zero position of these angles. The shortest footprint for an expansion ratio of 14.0 is obtained with Φ at 34° and Ψ between 10° and 15°. In most cases, the measured values in Figure 4 agree with the calculated predictions to within 5 percent, which is on the order of the accuracy of the measurements. The main point of Figure 4 is to show how easy it is to change the shape of the extremely elongated parallelogram (second image from the top) to the compact near-rectangle in the last image: this change in shape requires only a relatively coarse adjustment of the angle Ψ.

Figure 5 shows experimental results obtained with an APS-undulator-shaped x-ray beam, 1 mm high and 2 mm wide, with an energy of 8 keV (Bragg angle, θ_B = 14.2°), as one changes Φ, with Ψ fixed at 13°. Again, the error in the values of Φ and Ψ is ± 1°. Because of the uncertainty in the zero position of these angles, the starting values of Φ and Ψ were determined from the shape of the first image. The change in the angle was then taken from the change in the corresponding rotational stage dial reading, to the nearest degree. Note that the extra length L_S that is added by the parallelogram shape (sloping ends) does not add much to the overall length of the footprint. This means that Ψ need not be varied during the experiment as the footprint size is changed and/or as the energy of the beam is changed.

Figure 6 shows the expected shape of the footprint of an undulator-type x-ray beam, 1 mm high by 2 mm wide, as a function of the energy of the diffracted x-ray beam, from 5.7 keV to 51.3 keV. The calculations in Figure 6 show that the

contribution due to the slanted ends of the footprint does not alter significantly the total length of the footprint as the energy of the diffracted x-ray beam is changed. For all cases, Ψ is fixed at 12°, and R, the increase in footprint area relative to the incident beam area, is held close to 50 by adjusting Φ. The length L_S does not contribute more than 10 mm to the overall length for energies above 6.3 keV. To operate at lower energies, it may be necessary to readjust Ψ if the crystal is too short for the resulting footprint lengths (e.g. 64 mm). It is important to note that, if the crystal can accommodate a 64-mm-long footprint, the full range from 5.7 keV to 51.3 keV can be covered without changing Ψ , while achieving large expansion ratios for the area of the beam footprint, for example R = 50 in most cases.

Figure 7 shows a similar calculation for an APS-like wiggler-shaped beam, 2.3 mm high and 40 mm wide, in which Ψ = 13° and R is held close to 25 by adjusting Φ. The energy of the diffracted x-ray beam ranges from 6.3 keV to 26.9 keV. In this case, the extra length L_S, which is added to the length of the footprint in the direction of the beam by the sloping sides of the footprint, does make a significant contribution to the overall length of the footprint ($L_0 + L_S$) and will require the use of a larger crystal, about 150 mm long, if Ψ is not allowed to vary. Adjusting Ψ at any of the energies shown can reduce the length of L_S and make the use of a larger crystal unnecessary. Many experiments will not need this large an energy range, and thus a 60- to 100-mm-long crystal will be sufficient, if the value of Ψ is adjusted for different experiments at different energies.

ANGLE AND ENERGY ACCEPTANCE

The angle acceptance and the energy bandwidth of the asymmetric-cut monochromator can be varied by changing the angle Φ, the rotation around the axis perpendicular to the crystalline planes. This changes the incident angle γ of the x-ray beam on the surface of the crystal, the effective asymmetric-cut angle α_B, and the value of the parameter b, where $b = \sin(\theta_B - \alpha_B) / \sin(\theta_B + \alpha_B)$. The shape of the

beam is also changed.[7] The vertical height H_{bp} is increased over the height of the incident beam H_s by a factor of 1/b as is shown in Figure 8. The angular acceptance of the first crystal for diffraction of a monochromatic beam varies to first order as $1/(b)^{0.5}$. The angular emittance of the first crystal varies to first order as $(b)^{0.5}$ for a monochromatic beam. Thus, the ratio of the angular emittance of the diffracted beam to the angular acceptance of the incident beam is given by the value of b.[7]

As the x-ray beam is spread out on the surface of the crystal by the rotation around the $\hat{\Phi}$ axis, the value of b decreases, and the acceptance of monochromatic radiation increases. The larger angular acceptance can result in a major increase in the throughput of x-rays in the monochromator. Figure 9 illustrates this increase in the intensity of the diffracted beam as the acceptance angle increases for positive values of Φ, for data taken with the Cu K-$M_{II}M_{III}$ x-ray doublet. This overlapping doublet provided a source with a larger energy spread than was available with one of the single K-L lines. The intensity of the diffracted beam from the first crystal (filled circles) and the intensity of the diffracted beam from the second crystal (open squares) are plotted as a function of the angle Φ, with Ψ fixed at 14°. At Φ = 40°, the intensity of the diffracted beam from the first crystal increases by a factor of 2.5 over the measurement for Φ = 0°. With Φ = 35° for both crystals, about 80 percent of the diffracted beam from the first crystal is recovered by the second crystal. Further improvement in this recovery ratio is obtained by reducing the value of Φ for the second crystal, which increases the acceptance of the second crystal and brings the recovery of the intensity of the first crystal by the second crystal to almost 100 percent. This effect is illustrated in Figure 9. The open circle data points at Φ = 30° and 35° are the intensities of the diffracted beam from the second crystal when the value of Φ for the second crystal is reduced from 30° to 23° and from 35° to 26°, respectively. This control over the acceptance angle and emittance angle of the two crystals can be used to vary the monochromatic nature of the output beam as well as

its size, shape, angular divergence, and intensity.

VERTICAL WALK

Figure 10 shows how the use of asymmetric-cut crystals can reduce the vertical walk of the diffracted beam from the second crystal as compared to a normal double-crystal monochromator. The calculations of the vertical displacement of the diffracted beam from the second crystal versus the angle θ_B were performed for an offset between the two crystals of X_0 = 20 mm. The two curves are normalized so that zero vertical displacement occurs at 8 keV, θ_B = 14.2°, with an area expansion ratio of R= 25. The vertical walk for the asymmetric monochromator, for angles ± 5° around θ_B = 14.2°, is only 10 to 20 percent of the displacement calculated for the normal symmetric-cut monochromator. This effect occurs because the exit angle of the x-ray beam relative to the surface of the second crystal is much less in the asymmetric case than in the symmetric case. The walk along the surface of the second crystal is also less. This much reduced vertical walk for the asymmetric configuration has two advantages over the normal geometry. First, it allows for a larger rotation in θ_B before a translation of the second crystal is required to correct for the vertical displacement of the beam. Second, the vertical displacement adjustment is less sensitive to errors in the translation of the second crystal along the beam direction.

HORIZONTAL WALK

Horizontal walk occurs when the crystal is rotated about the $\hat{\Psi}$ axis. Due to this horizontal walk, the second crystal has to be adjusted in the direction perpendicular to the beam if one wishes to keep the footprint in the center of the second crystal when changing the value of Ψ. In most cases, one sets Ψ at an optimum angle and does not change it during the experiment. Figures 5-7 illustrate cases in which Ψ is held constant during the experiment or the calculation. If there is any horizontal walk from any other source, then it can be corrected by adjusting the angle Ψ.

References

1. R. K. Smither, G. A. Forster, C. A. Kot, and T. M. Kuzay, Liquid Gallium Metal Cooling for Optical Elements with High Heat Loads, Nucl. Instrum. Meth. **A266** (1988) 517-524.

2. R. K. Smither, G. A. Forster, D. H. Bilderback, M. Bedzyk, K. Finkelstein, C. Henderson, J. White, L. E. Berman, P. Stefan, and T. Oversluizen, Liquid Gallium Cooling of Silicon Crystals in High Intensity Photon Beams, Rev. Sci. Instrum. **60** (1989) 1486-1492.

3. R. K. Smither, Use of Liquid Metals as Cooling Fluids, Workshop on High Heat Load X-Ray Optics, ANL/APS/TM-6 (Aug. 1989) 83-131.

4. R. K. Smither, W. Lee, A. Macrander, D. Mills, and S. Rogers, Recent Experiments with Liquid Gallium Cooling of Crystal Diffraction Optics, paper presented at the 4th International Conference on Synchrotron Radiation Instrumentation, July 15-19, 1991, in Chester, England. Rev. Sci. Instrum. **63** (1992) 485, and Rev. Sci. Instrum., **63** (1992) 1746-1754.

5. W. K. Lee, A. T. Macrander, D. M. Mills, C. S. Rogers and R. K. Smither, Performance of a Gallium-Cooled 85° Inclined Silicon Monochromator for a High Power Density X-Ray Beam, Nucl. Instrum. & Meth. Phys. Res. **A320** (1992) 381-387.

6. P. J. Viccaro, Power Distribution from Insertion Device Synchrotron X-Ray Sources, SPIE 1990 Intl. Symposium on Opt., 7/90, San Diego, CA

7. T Matsushita and H. Hashizume, "X-Ray Monochromators," Chapter 4 of the *Handbook of Synchrotron Radiation,* Vol. 1, edited by E. E. Koch, North-Holland Publishing Co., 1983.

Figure Captions

Figure 1. Schematic drawing of an asymmetric-cut crystal showing three axes of rotation and associated angles, for the special case when $\Psi = 0$. For clarity, the crystal is shown as a square section of the round crystal that was used in the experiment. The crosshatched area is the footprint of the beam on the surface of the crystal.

Figure 2. Schematic drawing of the experimental setup showing the three axes of rotation and the two positions of the detector.

Figure 3. Schematic drawing of an asymmetric-cut crystal showing three axes of rotation and associated angles, for the general case when Ψ is not equal to zero. The crosshatched area is the footprint of the beam on the surface of the crystal.

Figure 4. Experimentally observed shapes of the x-ray beam footprint of a wiggler-like beam on the asymmetric-cut crystals with variation of Φ and Ψ. Initial beam and final beam profiles, 4 mm high and 12 mm wide, are shown on the left.

Figure 5. Experimentally observed shapes of the x-ray beam footprint of an undulator-like beam on the asymmetric-cut crystals with variation of Φ, with Ψ held constant at 13°. Initial beam and final beam profiles, 1 mm high and 2 mm wide, are shown on the left.

Figure 6. Calculated variation of the size and shape of the footprint for an undulator-shaped beam, 1 mm high and 2 mm wide, with changes in energy and Bragg angle, with the necessary adjustment of Φ to keep the increased area ratio, R, near 50, and with Ψ fixed at 12°.

Figure 7. Calculated variation of the size and shape of the footprint for a wiggler-shaped beam, 2.3 mm high and 40 mm wide, with changes in energy and Bragg angle, with the necessary adjustment of Φ to keep the increased area ratio, R, near 25, and with Ψ fixed at 13°.

Figure 8. Schematic view of the asymmetric-cut two-crystal monochromator, showing the variation in size of the diffracted beam as it passes through the spectrometer.

Figure 9. The measured intensity of the diffracted beam from the first crystal (open squares) and the second crystal (solid circles) as a function of Φ for the Cu K-$M_{II}M_{III}$ doublet, for the case when Ψ = 14°. Open circles are the intensities of the diffracted beam from the second crystal when the value of Φ is changed from 35° to 23° and from 40° to 26° for the points at Φ equal to 35° and 40°, respectively.

Figure 10. Comparison of the calculated vertical walk of a normal two-crystal monochromator with that of the asymmetric-cut two-crystal monochromator as the Bragg angle is changed. The two curves are normalized at θ_B = 14.2°.

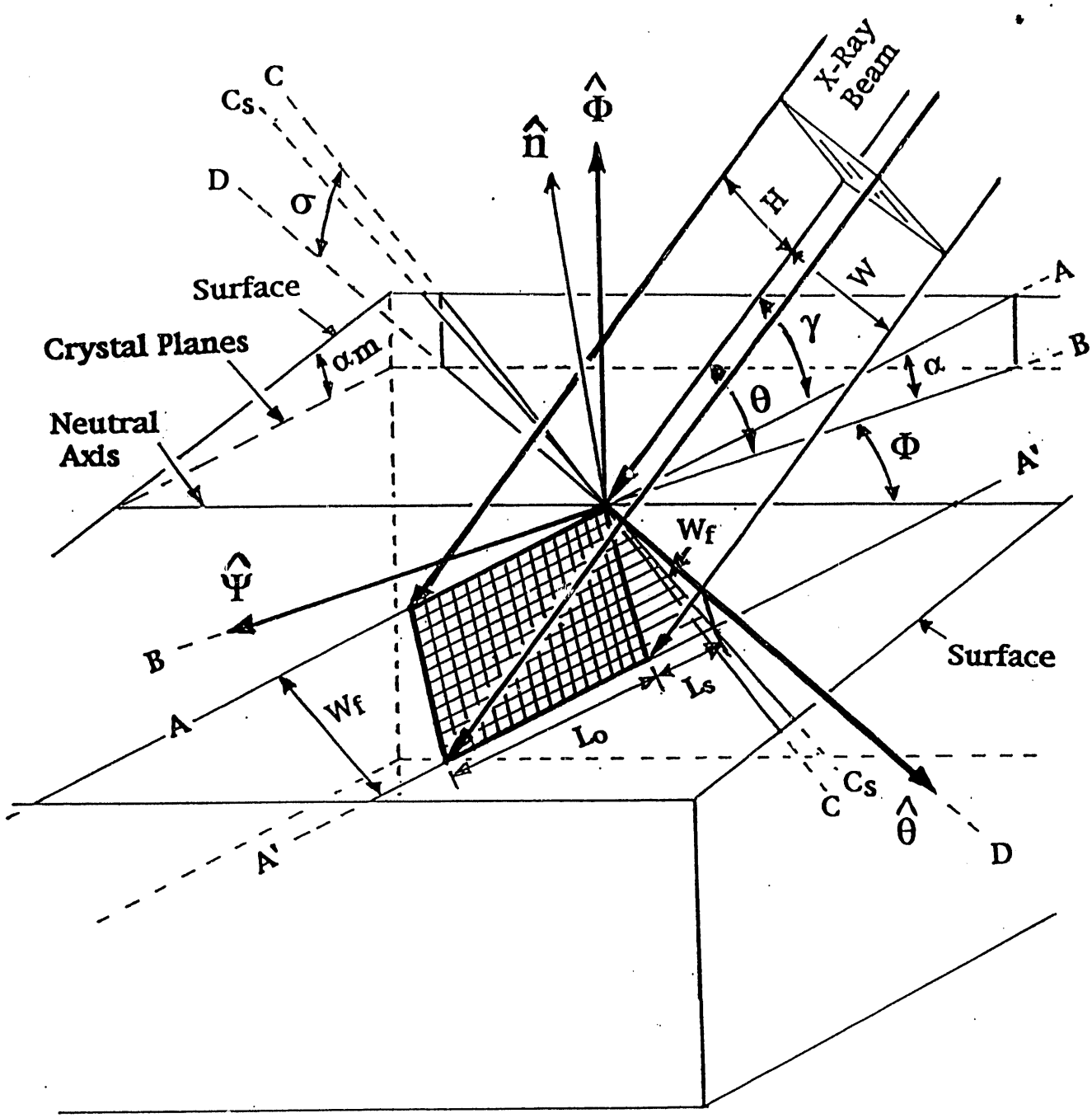
C
Cs
D
σ
n̂
Φ̂
X-Ray Beam
H
W
γ
A
B
Surface
Crystal Planes
αm
α
θ
Φ
A'
Neutral Axis
Wf
Ψ̂
B
A
Wf
Ls
Lo
Surface
Cs
C
θ̂
D
A'

FIGURE 1

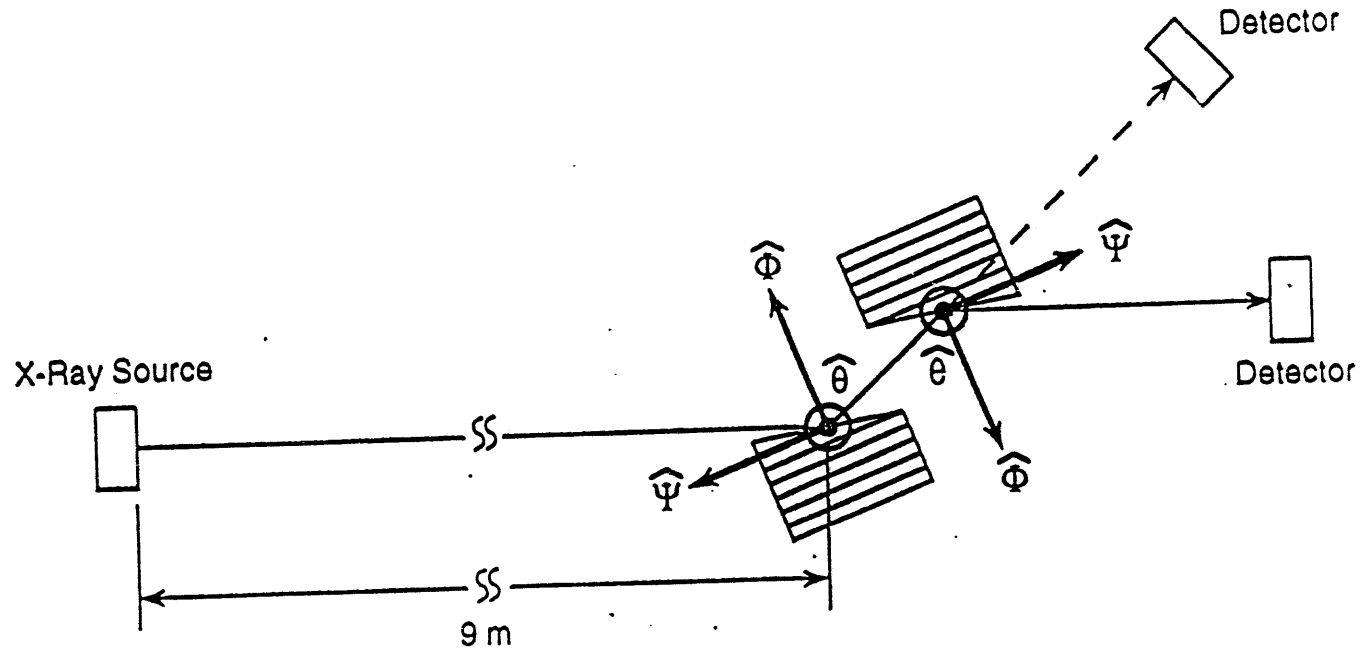

FIGURE 2

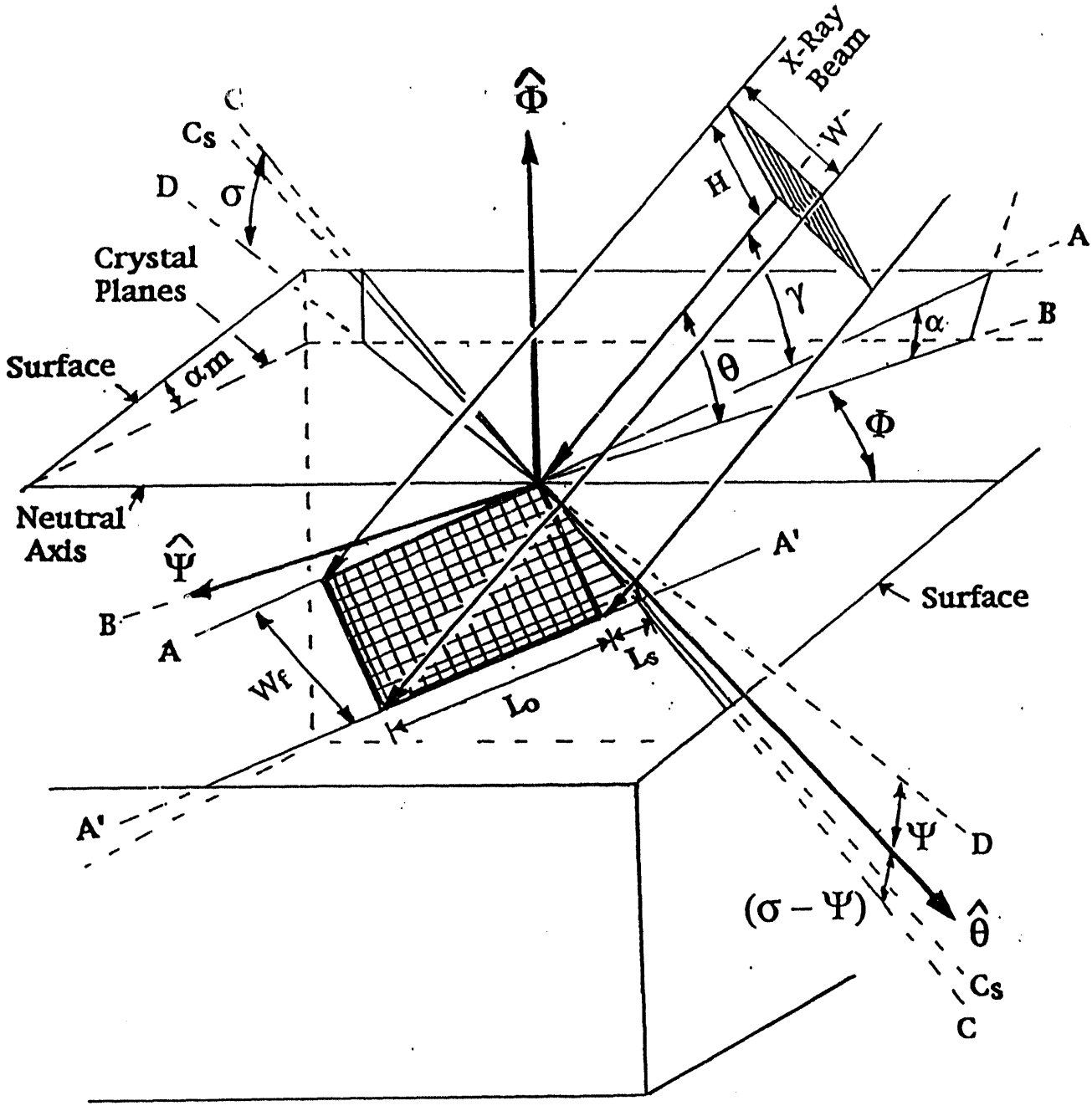
C
Cs
D
σ
Crystal Planes
Surface
α·m
Neutral Axis
Ψ̂
B
A
Wf
Lo
Ls
A'
Φ̂
X-Ray Beam
W
H
γ
θ
α
A
B
Φ
A'
Surface
Ψ
D
(σ − Ψ)
θ̂
Cs
C

FIGURE 3

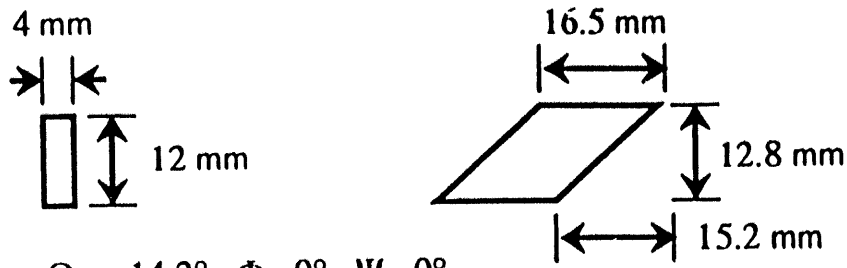

$\Theta_B = 14.2°$, $\Phi = 0°$, $\Psi = 0°$

AREA RATIO = 4.4 : 1
LENGTH = 31.7 mm

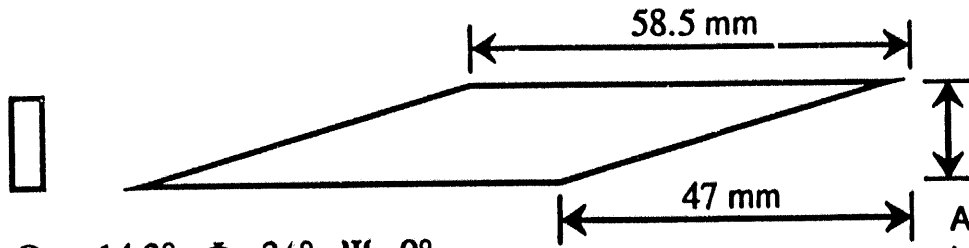

$\Theta_B = 14.2°$, $\Phi = 34°$, $\Psi = 0°$

AREA RATIO = 15.5 : 1
LENGTH = 105.5 mm

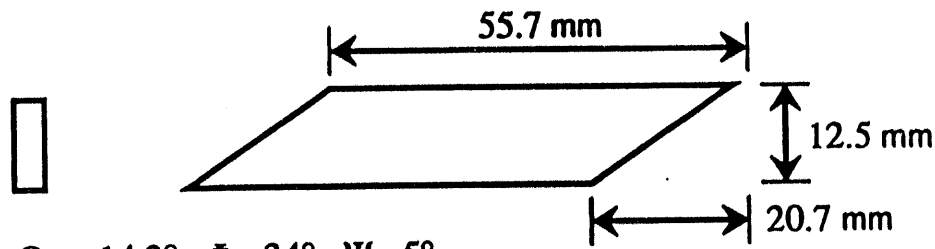

$\Theta_B = 14.2°$, $\Phi = 34°$, $\Psi = 5°$

AREA RATIO = 14.5 : 1
LENGTH = 76.4 mm

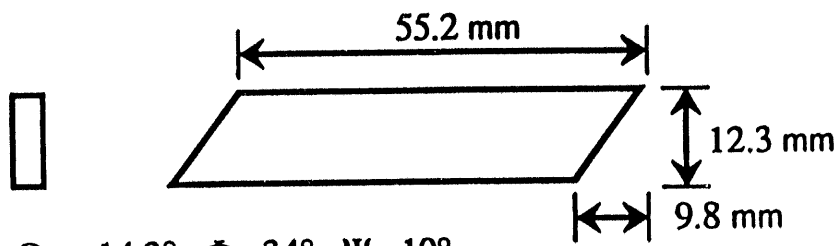

$\Theta_B = 14.2°$, $\Phi = 34°$, $\Psi = 10°$

AREA RATIO = 14.1 : 1
LENGTH = 65 mm

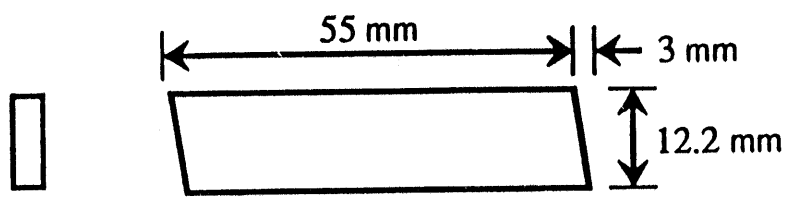

$\Theta_B = 14.2°$, $\Phi = 34°$, $\Psi = 15°$

AREA RATIO = 14.0 : 1
LENGTH = 58 mm

FIGURE 4

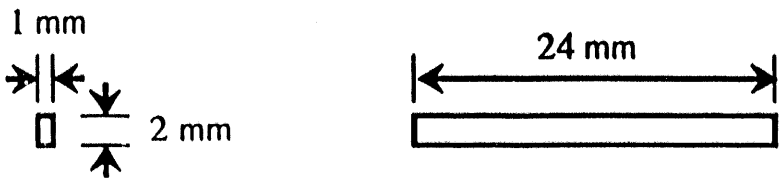

$\Theta_B = 14.2°$, $\Phi = 43°$, $\Psi = 13°$

AREA RATIO = 24 : 1
LENGTH = 24 mm

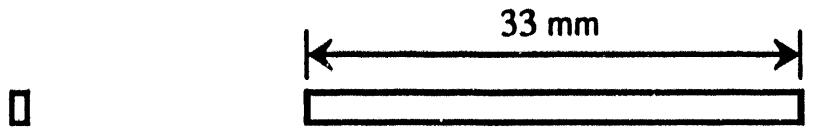

$\Theta_B = 14.2°$, $\Phi = 46°$, $\Psi = 13°$

AREA RATIO = 33 : 1
LENGTH = 33 mm

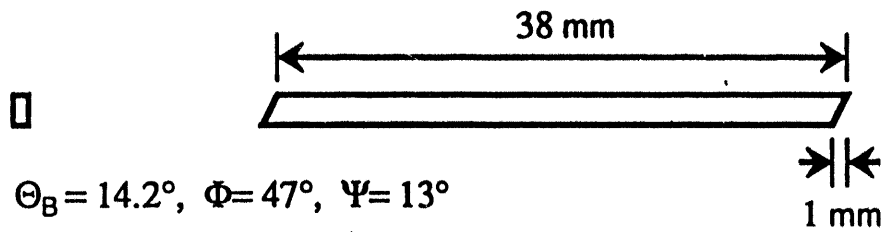

$\Theta_B = 14.2°$, $\Phi = 47°$, $\Psi = 13°$

AREA RATIO = 38 : 1
LENGTH = 39 mm

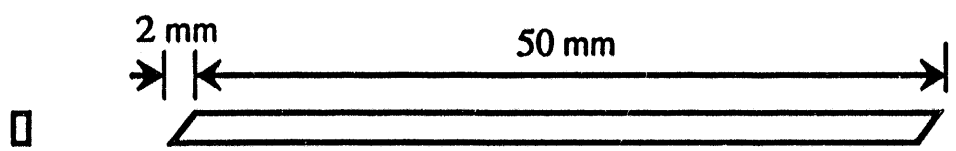

$\Theta_B = 14.2°$, $\Phi = 49°$, $\Psi = 13°$

AREA RATIO = 50 : 1
LENGTH = 52 mm

Θ_B	ENERGY		Φ	$L_0 + \|l_{-s}\|$	R
2.2°	51.3 keV	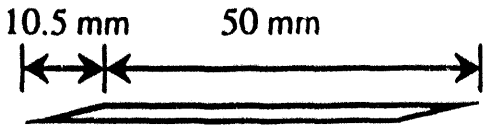	3.6°	60.5 mm	50.2
4.2°	26.9 keV		10.2°	60.0 mm	50.2
6.2°	18.2 keV	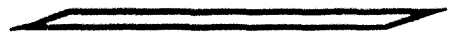	17.0°	59.2 mm	50.1
8.2°	13.8 keV		24.0°	57.9 mm	50.1
10.2°	11.1 keV	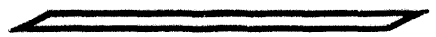	31.6°	56.1 mm	50.1
12.2°	9.3 keV		39.4°	53.6 mm	50.0
14.2°	8.0 keV	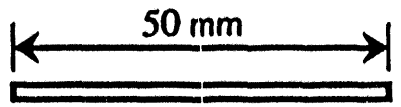	48.5°	50.3 mm	50.0
15.2°	7.5 keV		53.7°	51.9 mm	50.0
16.2°	7.1 keV		59.7°	54.7 mm	50.0
17.2°	6.7 keV	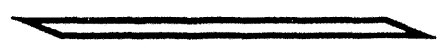	66.7°	57.8 mm	50.1
18.2°	6.3 keV	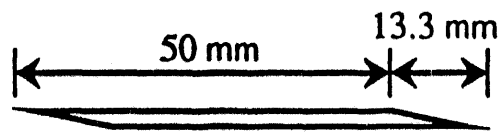	77.4°	63.3 mm	50.2
19.2°	6.0 keV	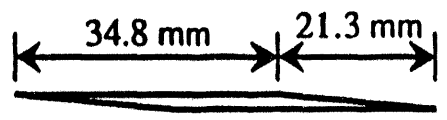	90.0°	56.1 mm	35.6
20.2°	5.7 keV	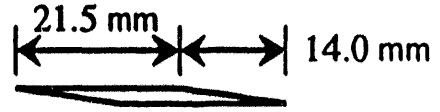	90.0°	35.5 mm	21.9

FIGURE 4

Θ	ENERGY		Φ	$L_0 + \|L_S\|$	R
4.2°	26.9 keV	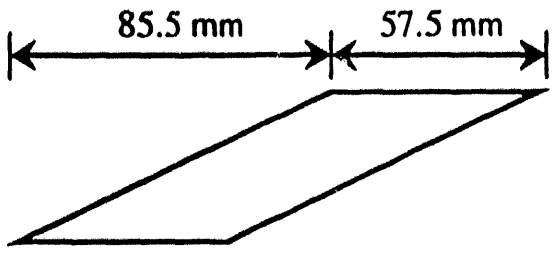	6.5°	143.0 mm	25.1
8.2°	13.8 keV	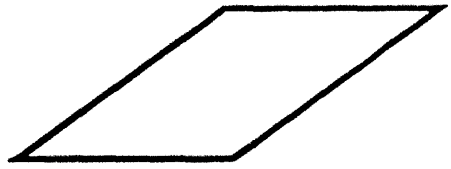	20.2°	126.1 mm	25.1
12.2°	9.3 keV	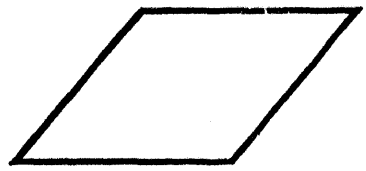	35.1°	89.8 mm	25.0
14.2°	8.0 keV	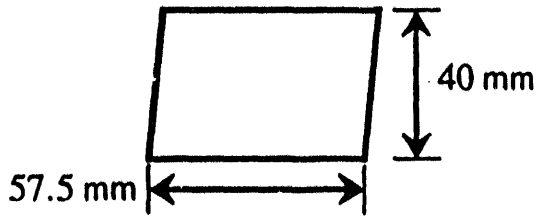	43.5°	61.4 mm	25.0
16.2°	7.1 keV	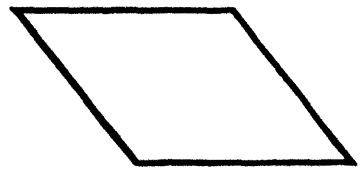	53.3°	91.4 mm	25.0
17.2°	6.7 keV	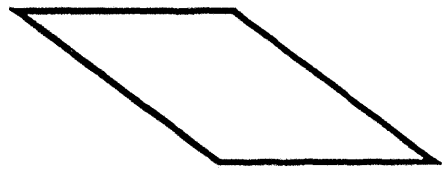	58.9°	116.1 mm	25.0
18.2°	6.3 keV	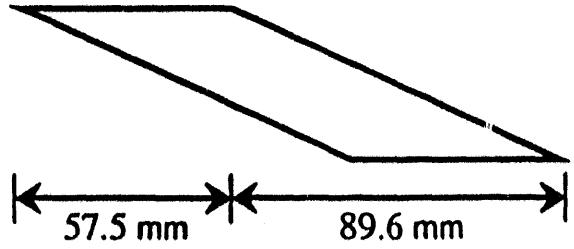	65.4°	147.1 mm	25.1

FIGURE 7

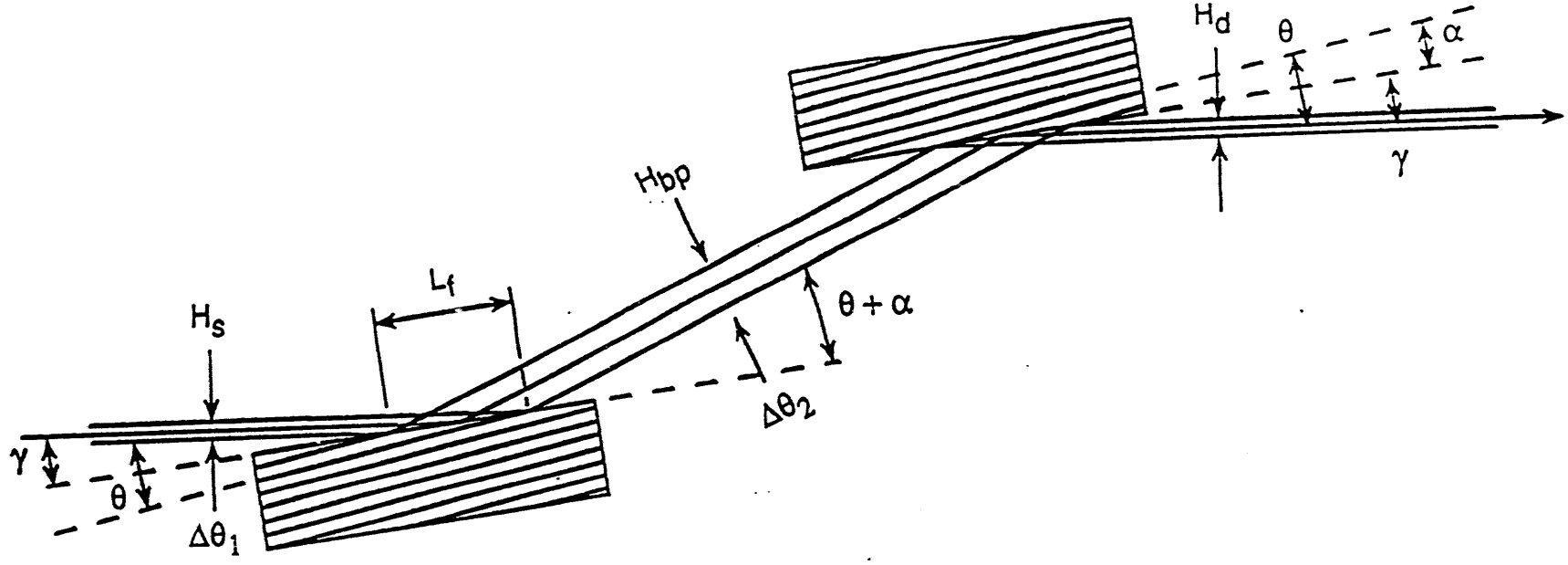

FIGURE 8

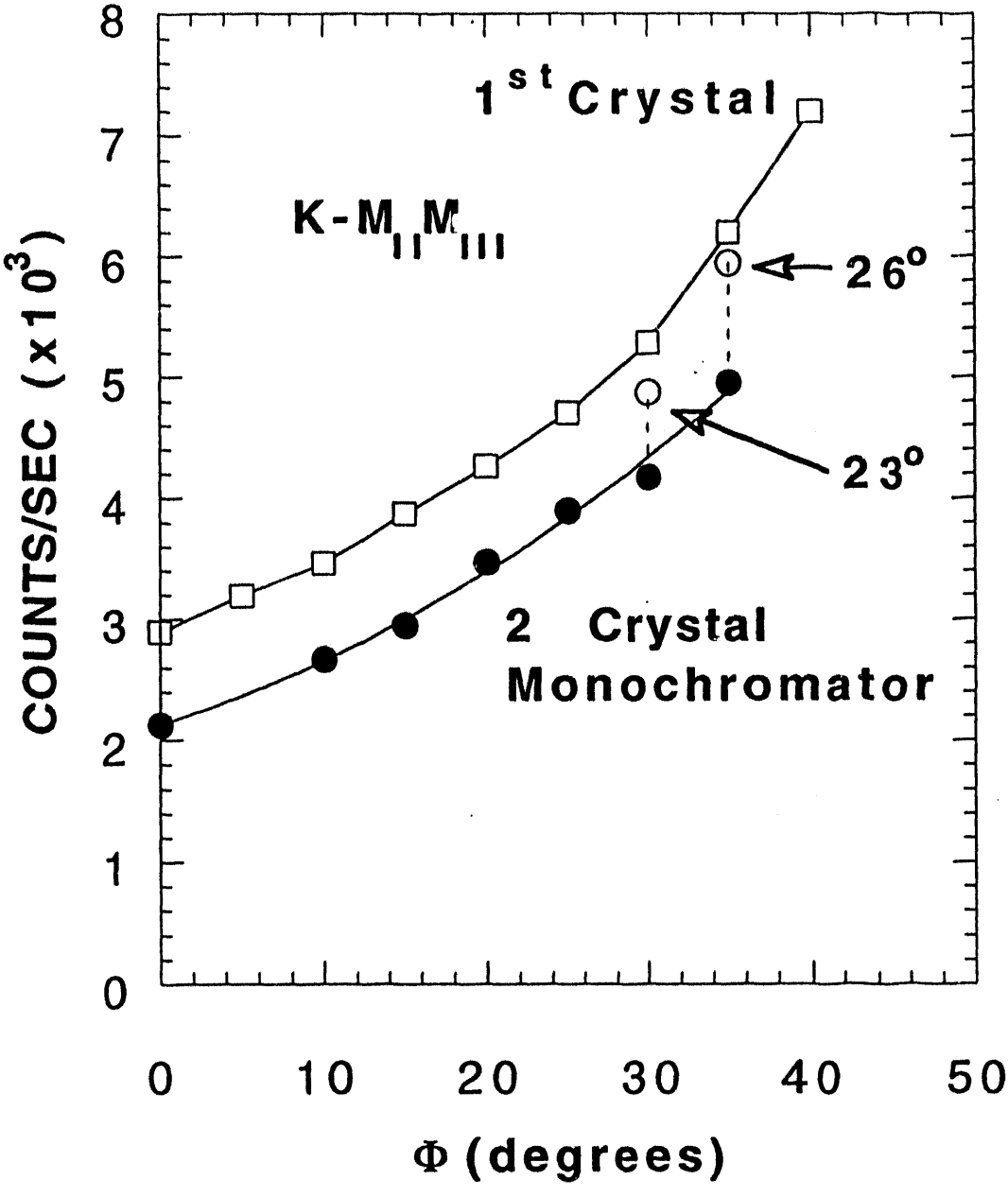

Rotation about axis ⊥ to crystalline planes

FIGURE 9

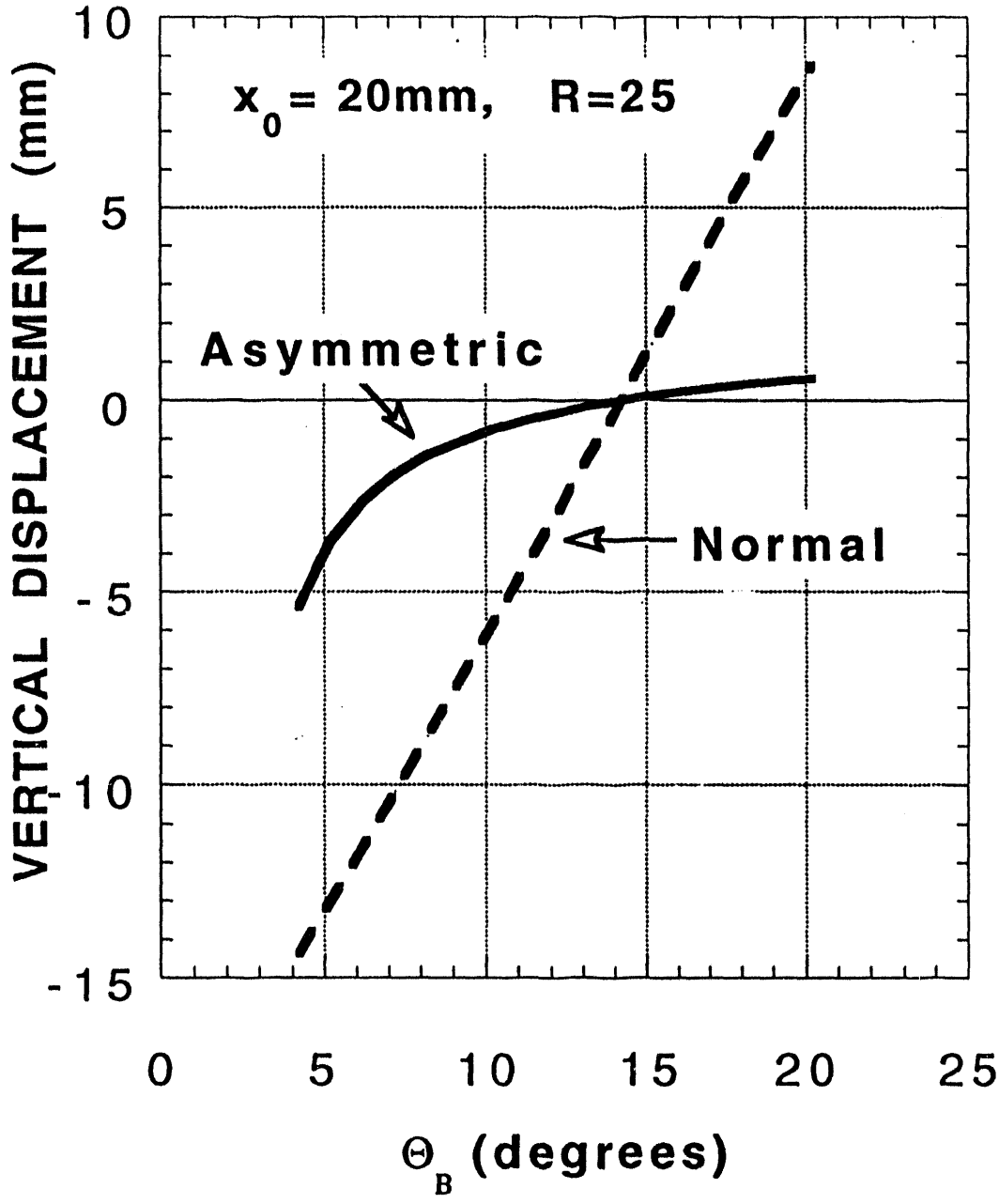
10
5
0
-5
-10
-15
VERTICAL DISPLACEMENT (mm)
x_0= 20mm, R=25
Asymmetric
Normal
0
5
10
15
20
25
Θ_B (degrees)

FIGURE 10

DATE
FILMED
10/11/94
END